JOURNAL OF SPACECRAFT AND ROCKETS
Vol. 38, No. 2, March–April 2001

Plume-On Base Drag Prediction Including Three-Dimensional and Real-Gas Effects

G. Rubio,* A. Matesanz,† and A. Velázquez‡
SENER Ingeniería y Sistemas, S.A., 28760 PTM-Tres Cantos, Madrid, Spain

A multicomponent method to predict base drag in base flow/plume interaction problems has been formulated, implemented, and validated. The formulation accounts for real-gas effects in the nozzle and in the plume as well as for three-dimensional effects associated with small angle of attack (up to 10 deg) conditions. Its application is intended for both launcher configuration analysis and missile drag prediction. Development of this methodology has been carried out to fill in the category of tools that are located between semi-empirical methods and computational fluid dynamics (CFD) algorithms. The technique being used consists of dividing the flowfield into several subregions that are solved separately and, subsequently, matched together in an iterative self-consistent way. Validation of the method has been performed by comparing the multicomponent method results with experimental and CFD data in a series of cases.

Nomenclature

$A(x)$ = nozzle area as function of horizontal coordinate x, m^2
C_p = specific heat at constant pressure (depends on temperature), J/kgK
C_{qe} = dimensionless mass flow through separation line of external flow
C_{qj} = dimensionless mass flow through separation line of jet flow
L_e = length of separation line (external flow), m
L_j = length of separation line (jet flow), m
M_j = jet exit Mach number
M_{1e} = external flow Mach number before shock wave at reattachment
M_{2e} = external flow Mach number after shock wave at reattachment
M_{1j} = jet flow Mach number before shock wave at reattachment
M_{2j} = jet flow Mach number after shock wave at reattachment
M_∞ = incident Mach number
P = gas pressure inside the nozzle, Pa
P_b = base pressure, Pa
P_T = total pressure in the combustion chamber, Pa
P_{tj} = jet stagnation pressure, Pa
P_∞ = freestream static pressure, Pa
q_{me} = mass flow through separation line of external flow, kg/s
q_{mj} = mass flow through separation line of jet flow, kg/s
R = gas constant, J/kg · K
R_e = axisymmetric body radius, m
R_R = radial coordinate of reattachment point, m
R_S = sting radius (jet-off case), m
T = gas temperature inside the nozzle, K
T_T = total temperature in Vulcain combustion chamber, K
T_{throat} = gas temperature at the nozzle throat, K
u = gas velocity inside the nozzle, m/s
u_{throat} = gas velocity at the nozzle throat, m/s
x = spatial coordinate along the nozzle, m
α = angle of attack
γ = ratio of specific heats
θ = circumferential angle, deg
ν = Prandtl–Meyer angle, deg
ρ = gas density inside the nozzle, kg/m^3
ρ_T = total density in Vulcain combustion chamber, kg/m^3
ρ_{throat} = gas density at the nozzle throat, kg/m^3
φ_{eR} = angle between external flow and horizontal axis, deg
φ_{jR} = angle between jet flow and horizontal axis, deg
χ = correction term to apply to Korst[29] theory
ψ_e = angle between external flow and flow after the reattachment, deg
ψ_j = angle between jet flow and flow after reattachment, deg
ψ_k = Korst[29] reattachment angle, deg
ψ' = $\partial\psi/\partial C_q$

Received 30 June 2000; accepted for publication 8 December 2000.

*Fluid Mechanics Engineer, Aerospace Division; also Ph.D Student, Carlos III University, Butarque 15, 28911 Leganes-Madrid, Spain.
†Fluid Mechanics Engineer, Aerospace Division.
‡Aerothermodynamics Manager, Aerospace Division; also Associate Professor, Mechanical Engineering Department, Carlos III University, Butarque 15, 28911 Leganes-Madrid, Spain.

Introduction

DESPITE base flow/plume interaction being studied for decades, major issues still remain when dealing with space transportation system design. This is the reason why a dedicated base flow thematic area has been included in the ESA program FESTIP (Future European Space Transportation Investigations Program) Technology Developments in Aerothermodynamics for Reusable Launch Vehicles. In this program, supersonic wind-tunnel tests have been carried out, together with a numerical analysis campaign performed using computational fluid dynamics (CFD) and multicomponent methods. The work that is presented in this paper is related to the development and validation of the multicomponent method that was used in this ESA program.

Broadly speaking, a generic trend could be identified when looking at the extensive literature that is available in the field of base flow/plume interaction. In the 1960s and 1970s, a considerable amount of effort was dedicated to build up experimental databases and to correlate those data in a meaningful way. This effort gave rise to the generation of a number of semi-empirical methods characterized by their ability to perform vast parameter screenings at almost no computational cost. On the other hand, generalization of this approach has proved to be difficult outside the limits set up by the experimental conditions. A sample of these methods may be found in Refs. 1–6. In addition, a very comprehensive review has been published by Lamb and Oberkampf.[7]

Another set of methods for base drag prediction is based on a multicomponent formulation. Basically, these methods consist of dividing the flowfield into several regions that are solved separately and then coupled together in an iterative fashion by applying some compatibility conditions. Depending on the model used for each region and, also, on the degree of sophistication devoted to the coupling, different models arise. Historically, all of these methods derive from the developments made by Chapman and Korst,[8] Korst et al.,[9] and Korst[10] in the 1950s. Alber and Lees[11] proposed an alternative approach in 1968. Their methodology was based on an integral formulation, and they reported a good capability to predict

base flow pressures behind supersonic streams up to Mach 2.3. To our knowledge, this approach has not been further pursued.

In the context of the theory expounded in Refs. 8–10, Fox[12] presented improvements on the recompression model. Addy et al.[13] studied the effect of lack of symmetry in the nozzle contour of a thick missile base. In this paper, the authors reported that nonuniform effects might account for up to a 6% increase in base pressure. Schetz et al.[14] analyzed the base flow downstream of a missile moving at supersonic speeds with mass addition. The authors stated that they did not use the integral method described in Ref. 11 because of its complexity when trying to generalize to more complex situations. Weng and Chow[15] reported on the influence of the sting of the experimental model when studying axisymmetric flow past a thick backward facing step.

Tanner[16] discussed the thickness influence of the incoming boundary layer on base pressure. Another formulation, based on the method of characteristics for the external flow and the theory from Refs. 8–10 for the turbulent shear layers, to study base flows in the presence of an exhaust jet, has been described by Wagner and White.[17] The authors were able to match in a smooth way different flow models applied to different flowfield regions; the influence of the approaching boundary layer was introduced, and an improvement for the recompression model was proposed. More recently, Huang et al.[18] studied the internal flow downstream of a backward facing step by using a similar approach. In particular, the authors conclude that the method works quite satisfactorily up to the reattachment point. However, downstream of that point, a different approach, most likely CFD, has to be used. Also, comprehensive reviews of multicomponent methods have been published by Reijasse et al.,[19] Delery and Wagner,[20] and Jenn.[21]

In addition to semi-empirical and multicomponent methods, one has to refer to the large effort that is being carried out nowadays in the field of CFD analysis of base flows. Comparison of experimental vs numerical results, obtained by using two algebraic and by one $\kappa-\varepsilon$ turbulence model downstream of a cylindrical afterbody, immersed into a Mach 2.46 supersonic flowfield has been presented by Sahu.[22] In this case, the author reported poor prediction capabilities of both algebraic models when compared with the $\kappa-\varepsilon$ formulation. Another comparison, this time by using the low-Reynolds-number form of a standard two-equation model, a two layer algebraic stress model, and a Reynolds stress model, has been presented by Chuang and Chieng.[23] In their conclusions, the authors concluded that the best performance was obtained with the Reynolds stress model. Wang[24] computed a clustered nozzle configuration with four engines. Apart from the presentation of the computational results, the author discusses the physics of the reverse jet impinging on the base center. Recently, Sahu and Heavey[25] computed supersonic base flow over a cylindrical afterbody with base bleed.

The work that is presented in this paper evolves a multicomponent method toward including three-dimensional and real-gas effects. The reason, as pointed out by Delery and Wagner[20] in Sec. 2 of their review paper, is that there is still room for improving multicomponent methods. In particular, this is true with regard to increasing their range of applicability because most of the existing multicomponent methods are axisymmetric and have a limited treatment of real-gas effects. Nevertheless, it could be argued that the most promising way to proceed is to concentrate the development effort on CFD algorithms. This approach was followed by Dash and Sinha[26] with their formulation of zonal methods. In particular, these authors divide the flowfield into a series of different computational domains and are able to apply very sophisticated CFD modeling to each of them. For example, plume thermochemistry with nonequilibrium effects, two-phase flow, and turbulence can be treated with good accuracy. Also, the outright CFD approach, as has been done by Sillen,[27] can also be applied to the simulation of launcher base flow/plume interaction problems including real-gas effects.

In any case, CFD methods rely on accurate turbulence modeling, and this subject still needs significant improvement when large regions of separated flow are present in the flowfield. In particular, the authors of this paper have recently experienced the difficulties of the CFD approach[28] when implementing an explicit algebraic Reynolds stress model (EARSM) within a three-dimensional finite element method to predict massively separated flow behavior. Furthermore, we believe that the CFD and the multicomponent approach are not incompatible inasmuch as significant gains can be obtained when using these two approaches in a cooperative way. For instance, a multicomponent solution may provide a good startup flowfield for a time-marching CFD algorithm. Also, a reliable multicomponent method could be used to do extensive parameter surveys to discard unfeasible combinations, thus focusing CFD on those cases of actual interest.

The multicomponent method that is formulated and validated in the remainder of this paper has been developed in a steplike fashion as follows: 1) axisymmetric, 0-deg angle of attack, perfect gas; 2) axisymmetric, 0-deg angle of attack, real gas; 3) three-dimensional, up to 10-deg angle of attack, perfect gas; and 4) three-dimensional, up to 10-deg angle of attack, real gas.

In the following sections, the different steps are formulated and results of the validation study are given. Finally, conclusions are presented.

Formulation of Steps 1 and 2

In what follows, the flow domain is divided into five different regions: 1) inviscid supersonic external flow, 2) inviscid supersonic nozzle flow, 3) base cavity, 4) mixing layer located between regions 1 and 3 and regions 3 and 5, and 5) inviscid supersonic jet flow. This topology is presented in Fig. 1.

Concerning the calculation algorithm, the following sequence is followed:

1) An arbitrary value for the base pressure in the cavity (region 3) is assumed.

2) Region 1 (inviscid supersonic external flow) is computed by using the method of characteristics. The ideal extent of the outward facing mixing layer is obtained as a function of the assumed base pressure.

3) Region 2 (inviscid supersonic nozzle flow) is computed by solving the quasi-one-dimensional nozzle flow equations including real-gas effects (C_p is a function of the temperature) whenever applicable.

4) Region 5 (inviscid supersonic jet flow) is computed by using the method of characteristics including real-gas effects (C_p is a function of the temperature) whenever applicable.

5) Turbulent effects are introduced in the problem through both mixing layers (region 4). To get an accurate description of the mixing process, a semi-empirical correlation is used. This correlation, based on the angular reattachment criterion,[29] allows for the computation of the net mass flow into the cavity, and is corrected whenever γ differs from 1.4.

6) The process is repeated in an iterative fashion until the net computed mass flow into the base cavity (region 3) is zero.

The formulation of the different regions is as follows.

For region 1, an Euler algorithm is used to compute the forebody flowfield up to the shoulder of the geometry under consideration. Then, a standard axisymmetric method of characteristics is used for the afterbody flow.

For region 2, equations that govern the quasi-one-dimensional flow inside the convergent–divergent nozzle with variable C_p are as follows:

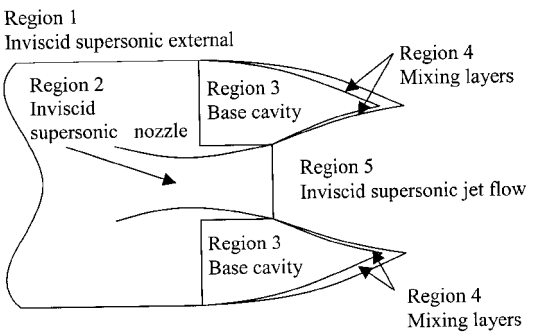

Fig. 1 Topology of the problem.

$$\frac{\mathrm{d}}{\mathrm{d}x}(\rho u A) = 0 \tag{1}$$

$$\rho u \frac{\mathrm{d}u}{\mathrm{d}x} = -\frac{\mathrm{d}P}{\mathrm{d}x} = -R \cdot \left(\rho \frac{\mathrm{d}T}{\mathrm{d}x} + T \frac{\mathrm{d}\rho}{\mathrm{d}x}\right) \tag{2}$$

$$\frac{\mathrm{d}}{\mathrm{d}x}\left(C_p T + \frac{u^2}{2}\right) = 0 \tag{3}$$

where C_p depends nonlinearly on the temperature. Furthermore, in the cases to be considered, the gas constant R can be assumed to be constant. The main problem associated with the numerical solution of Eqs. (1–3) is the presence of a singularity at the nozzle throat. To overcome this circumstance, flow variables are perturbed in the neighborhood of the throat as follows:

$$\rho = \rho_{\text{throat}} + \lambda_1 \cdot z \tag{4}$$

$$u = u_{\text{throat}} + \lambda_2 \cdot z \tag{5}$$

$$T = T_{\text{throat}} + \lambda_3 \cdot z \tag{6}$$

where λ_1, λ_2, and λ_3 are the slopes, to be determined, of the trajectories leading out of the saddle point singularity existing at the nozzle throat and z is the spatial coordinate along the throat. Then, the computation algorithm proceeds sequentially as follows: 1) ρ_{throat} and T_{throat} are arbitrarily chosen; 2) u_{throat} is obtained by requiring that derivatives of the flow variables are finite at the throat; 3) flow variables are perturbed in the fashion shown in Eqs. (4–6), and the slopes λ_1, λ_2, and λ_3 of the trajectories leading out of the saddle point at the throat are obtained as a function of ρ_{throat}, u_{throat}, and T_{throat}; 4) Eqs. (1–3) are integrated upstream from the throat to the entrance section of the nozzle (combustion chamber); 5) the integration process is iteratively repeated (by changing T_{throat} and ρ_{throat}), until the combustion chamber conditions are met at the entrance section of the nozzle; and 6) once the correct T_{throat} and ρ_{throat} are known, Eqs. (1–3) are integrated downstream from the throat up to the final section of the divergent part of the nozzle.

Equations (1–3) could, of course, be integrated in a different fashion, for example, by including time-dependent terms and applying a time-marching algorithm. However, the method just described, which is standard for this type of equation, proves to be very robust and time efficient. For the sake of completion, the relation that links T_{throat} and u_{throat} is

$$\frac{u_{\text{throat}}^2}{C_0 \cdot T_T} = \frac{T_{\text{throat}}}{T_T} \times \frac{\left[1 + k_1 (T_{\text{throat}}/T_T) + k_2 \left(T_{\text{throat}}^2/T_T^2\right)\right]}{\left[(C_0 - R)/R + (C_0 \cdot k_1/R)(T_{\text{throat}}/T_T) + (C_0 \cdot k_2/R)\left(T_{\text{throat}}^2/T_T^2\right)\right]} \tag{7}$$

and the slopes λ_1, λ_2, and λ_3 of the trajectories are given by

$$\lambda_2 = \left[\frac{\delta_2}{P_2 - (\delta_3/\delta_2) \cdot P_3}\right]^{\frac{1}{2}} \tag{8}$$

$$\lambda_1 = -\frac{\delta_1}{\delta_2}\lambda_2 \tag{9}$$

$$\lambda_3 = -\frac{\delta_3}{\delta_2}\lambda_2 \tag{10}$$

where

$$P_2 = 2\frac{u_{\text{throat}}}{\sqrt{C_0 \cdot T_t}} \cdot \left(\frac{C_0 - R}{R} + \frac{C_0 \cdot k_1}{R}\frac{T_{\text{throat}}}{T_T} + \frac{C_0 \cdot k_2}{R}\frac{T_{\text{throat}}^2}{T_T^2}\right) \tag{11}$$

$$P_3 = \frac{u_{\text{throat}}^2}{C_0 \cdot T_T} \cdot \left[\frac{C_0 \cdot k_1}{R} + 2\frac{C_0 \cdot k_2}{R}\frac{T_{\text{throat}}}{T_T}\right] - \frac{T_{\text{throat}}}{T_T}\left[2k_1 + 3k_2\frac{T_{\text{throat}}}{T_T}\right] \tag{12}$$

$$\delta_1 = \frac{1}{\left(a_0/L^2\right)} 2a_1 \frac{\rho_{\text{throat}}}{\rho_T}\frac{u_{\text{throat}}^2}{C_0 T_T} \cdot \left[\frac{C_0 - R}{R} + \frac{C_0 k_1}{R}\frac{T_{\text{throat}}}{T_T} + \frac{C_0 k_2}{R}\frac{T_{\text{throat}}^2}{T_T}\right] \tag{13}$$

$$\delta_2 = \frac{1}{\left(a_0/L^2\right)} 2a_1 \frac{T_{\text{throat}}}{T_T}\frac{u_{\text{throat}}}{\sqrt{C_0 T_T}}\left[1 + k_1\frac{T_{\text{throat}}}{T_T} + k_2\frac{T_{\text{throat}}^2}{T_T^2}\right] \tag{14}$$

$$\delta_3 = \frac{1}{\left(a_0/L^2\right)} 2a_1 \frac{T_{\text{throat}}}{T_T}\frac{u_{\text{throat}}}{C_0 T_T} \tag{15}$$

$$k_1 = 2C_1/C_0 \tag{16}$$

$$k_2 = 3C_2/C_0 \tag{17}$$

where L is the length of the convergent part of the nozzle and a_0 and a_1 are the first and second coefficients of the Taylor expansion of the nozzle profile at the throat. C_0, C_1, and C_2 are the three terms of the polynomial approximation for C_p as a function of the total temperature, that is, $C_p = C_0 + C_1 T + C_2 T^2$.

For region 3, flow behavior in this dead air cavity is modeled assuming constant pressure.

For region 4, the empirical relations[19] that link dimensionless mass flows with other flow parameters are

$$\psi_e = \psi_k(M_{1e}) + \arctan\{\chi(M_{1e}) \cdot [(L_e/R_R)\sin\varphi_{eR} + 1]\} + C_{qe}\psi'(M_{1e}) \tag{18}$$

$$\psi_j = \psi_k(M_{1j}) + \arctan\{\chi(M_{1j}) \cdot [(L_j/R_R)\sin\varphi_{jR} + 1]\} + C_{qj}\psi'(M_{1j}) \tag{19}$$

where topology and parameters of the reattachment point region and base cavity (M_{1e}, L_e, R_R, φ_{eR}, ψ_e, M_{1j}, L_j, φ_{jR}, and ψ_j) are shown in Fig. 2. Dimensionless mass flows that go into the cavity are

$$C_{qe} = \frac{q_{me}}{2\pi R_R L_e \rho_e u_e} \tag{20}$$

$$C_{qj} = \frac{q_{mj}}{2\pi R_R L_j \rho_j u_j} \tag{21}$$

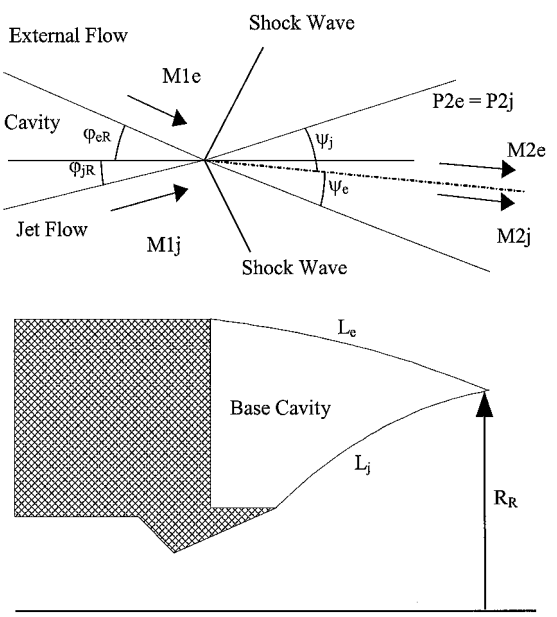

Fig. 2 Topology of the reattachment point region and base cavity.

Table 1 Comparison between experimental, CFD, and multicomponent method results: axisymmetric, perfect gas, plume-on case

$M_\infty = 1.96$, $M_j = 3.95$						$M_\infty = 2.98$, $M_j = 3.95$			
P_{tj}/P_∞	Experimental[32] P_b/P_∞	CFD[28] EARSM P_b/P_∞	Multi-component P_b/P_∞	CFD[28] EARSM error %	Multi-component error %	P_{tj}/P_∞	Experimental[32] P_b/P_∞	Multi-component P_b/P_∞	Multi-component error %
54.4	0.30	0.34	0.29	15	3	121.4	0.22	0.20	10
97.2	0.33	0.38	0.33	14	1	193.5	0.25	0.24	6
173.9	0.37	0.42	0.38	13	3	397.0	0.31	0.31	1
349.5	0.42	0.47	0.46	12	9	612.1	0.34	0.37	9

where q_{me} and q_{mj} are dimensional mass flows. Variables ψ_k, ψ', and χ are empirical functions of M_1 (Ref. 29).

To upgrade this formulation to account for variable γ effects, we gathered experimental data[19] and sought an empirical relation for the variables under consideration. In particular, the scaling law that we were able to construct is

$$\psi_k(\gamma, M) = \psi_k(1.4, M) \cdot \left\{1 + 0.81\left[\frac{\nu(\gamma, M)}{\nu(1.4, M)} - 1\right]\right\} \quad (22)$$

For region 5, the jet is computed by using a method of characteristics that accounts for variable γ effects. In practice, each downstream step is iterated until the flow variables are consistent with the local value of γ that is a function of temperature.

Formulation of Steps 3 and 4

Because of the complexity associated with the three-dimensional base flow problem, two different formulations have been developed. The first one refers to plume-off cases only, whereas the second one deals with base flow/plume interaction.

Plume-Off Formulation

The determination of base pressure in absence of a jet raises a specific problem with regard to the selection of criteria needed to close the formulation. In the purely axisymmetric case, mass flow through meridional z–r planes must be, because of symmetry, identical to that of the others. In the three-dimensional case, the situation is different because an azimuthal distribution of pressure exists on the base surface.

To deal with this problem, we have used the formulation of Mueller et al.[30] plus some additional corrections that we have developed to improve the results. Basically, the idea consists of assuming that the shear layers streaming from the base shoulder reattach at some virtual sting. In this idealization, the sting represents the core of the viscous wake that exists downstream of the cylindrical body. The correction that we propose for $0 \le \theta \le 90$ deg is (Fig. 3)

$$\Psi_e = \Psi_k \quad (23)$$

and for $90 \le \theta \le 180$ deg

$$\Psi_e = \Psi_k - \alpha \cdot \cos\theta \quad (24)$$

The argument that supports correction (24) is that the virtual sting associated with the Mueller et al. formulation should be aligned with the upstream flowfield when the angle of attack is other than zero. In the upper part of the base, if the flow separates before the base shoulder, the correction is not used.

Plume-On Formulation

In this case, local expansions are placed at every azimuthal position in the base shoulder. Formally, this approach assumes that the flow topology behaves in a quasi-axisymmetric way, and this limits the application of the method to small-angle-of-attack conditions. During the course of the validation study, we found that the method could be used up to angles of attack of the order of 10 deg. This means that the method is valid for typical missile trajectory computations, as well as for a significant range of angle of attack associated with launcher design. In this case, the formulation of step 1 is applied sequentially to azimuthal slices of finite width. However, formulation of the inviscid supersonic external flow, at least in the cases that have been chosen for validation purposes, has required the implementation of further improvements. The reason is that the experimental data used for validation, provided by Englert et al.,[31] refer to boattailed bodies that present a shock wave at the base shoulder; accordingly, this circumstance has been accounted for when modeling the external inviscid flow.

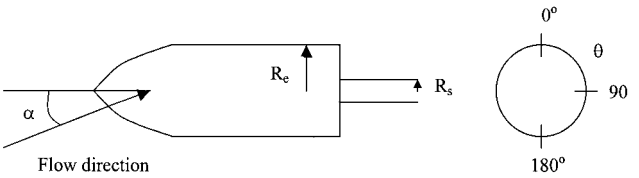

Fig. 3 View of the body with the fictitious sting.

Real-Gas Effects

Implementation of these effects is achieved by combining the three-dimensional methodology explained in the preceding section with the formulation developed for step 2.

Validation of Step 1

In this case, the multicomponent method has been validated first by comparing its results with plume-on experimental[32] and CFD data.[28] The experimental setup[32] is shown in Fig. 4. Mach numbers of the external flow were 1.96 and 2.98, and the exit Mach number of the nozzle flow was 3.95. Four different nozzle pressure ratios were tested in each case. The results are summarized in Table 1. Note that the uncertainty of the experimental results[32] is of the order of 2%. Also, the authors stated that the very thin model sting did not significantly affect base pressure.

The EARSM model[28] used with the CFD method data has evolved from a previous k–ε version developed by the same authors.[33] The EARSM computations that appear in Table 1 were carried out as follows: Blunted conical forebody and cylindrical afterbody were computed on a separate grid with the k–ε version of the solver. Then, shoulder flow profiles were implemented as boundary conditions for the EARSM base flow simulation. In particular, a three-dimensional mesh having 712,780 nodes was used in this domain. When looking at the results given in Table 1, note that the deviation between CFD computations and experimental results ($M_\infty = 1.96$) was of the order of 15%. However, for the range of parameters under consideration, the multicomponent method produced deviations ranging from 1 to 9%. Furthermore, note that only 1 min was needed on a Pentium®-based personal computer to obtain each of the multicomponent results. On the other hand, the error associated with the CFD computations consistently decreased when the nozzle pressure ratio increased, whereas the multicomponent error at first decreases, and then increases as the nozzle pressure ratio increases. For the cases with $M_\infty = 2.98$, no CFD data were available. When comparing with experimental results, the multicomponent errors were still less than 10%, their tendency being also consistent with the $M_\infty = 1.96$ cases; that is, the error has a minimum in the middle of the nozzle pressure ratio range, and increases afterwards.

For plume-off cases, three different sets of experimental results have been used for validation purposes. They include, again, the data of Bannink et al.[32] and the well-documented experiments of Herrin and Dutton on a cylindrical afterbody[34] and on a boattailed axisymmetric body.[35] In the case of the cylindrical afterbody,[34] Mach and Reynolds number per meter were 2.5 and 52×10^6, respectively,

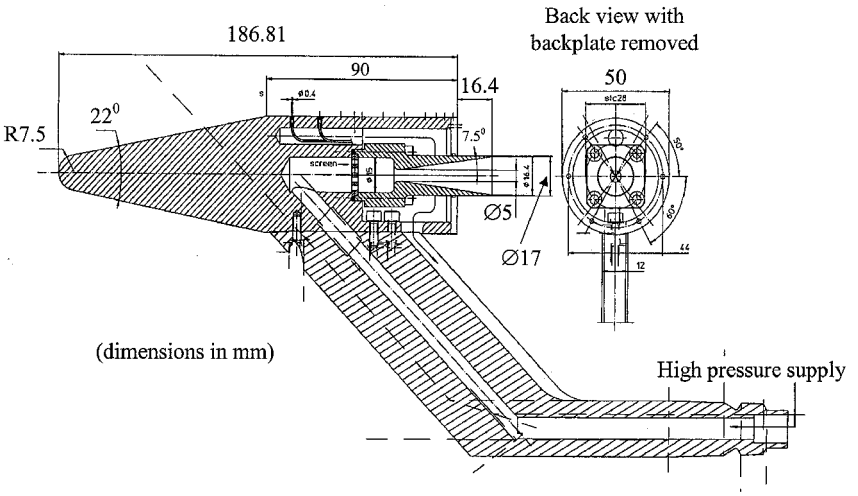

Fig. 4 Experimental setup (from Bannink et al.,[32] with permission).

Table 2 Comparison between experimental, CFD, and multicomponent method results: axisymmetric, perfect-gas, plume-off case

Experimental case	M_∞	Re, m^{-1}	P_b/P_∞, experimental	P_b/P_∞, multicomponent	Error, %
Cylindrical afterbody[32]	1.96	27.6×10^6	0.52	0.57	10
Cylindrical afterbody[32]	2.98	46.6×10^6	0.33	0.34	3
Cylindrical afterbody[34]	2.50	52.0×10^6	0.55	0.49	10
Boattailed cylinder[35]	2.46	52.0×10^6	0.63	0.56	11

whereas the cylinder diameter was 63.5 mm. In the case of the boattailed body, Mach and Reynolds number per meter were 2.46 and 52×10^6, respectively, cylinder diameter was 63.5 mm, and the boattail had an angle of 5 deg. The experimental uncertainty of these results[34,35] was 2%. The results obtained (in terms of P_b/P_∞) are presented in Table 2.

Validation of Step 2

The geometry that has been computed in this case (Fig. 5) consists of a forebody similar to that of Fig. 4 but scaled to 20.9 m from nose to base shoulder and fitted with a Vulcain nozzle. This configuration, which represents a generic reusable launch vehicle concept, has been studied within the scope of the ESA FESTIP program. External flow conditions were $M_\infty = 3$, altitude = 22 km, $Re_\infty = 8.4 \times 10^7$ (based on vehicle length), $P_\infty = 4000$ Pa, and $T_\infty = 219$ K. Vulcain engine combustion chamber conditions were O_2/H_2 mass ratio = 5.89, $P_T = 9466.8$ kPa, $\rho_T = 4.405$ kg/m^3, and $T_T = 3151$ K. Accordingly, the following C_p variation was chosen: $C_p(T) = 1985.5 + 0.9197 \cdot T - 1.1855 \times 10^{-4} \cdot T^2$ J/kg · K.

This case, for which there is no experimental data, has been computed by Sillen[27] using a CFD algorithm with a k–ε formulation for turbulence and a suitable model for plume thermodynamics effects. The axisymmetric grid contained 108,000 cells, and the normalized base pressure P_b/P_∞ computed by Sillen was 0.517. The multicomponent method result was 0.520, which is remarkably close to the CFD figure. Regarding computational time, the multicomponent method required 3 min of CPU time on a Pentium-based personal computer. Also, this case represents a good test to assess the capabilities of the multicomponent formulation. The reason is that, as pointed out by Delery and Wagner,[20] these methods tend to deteriorate when the nozzle exit diameter decreases. In the configuration shown in Fig. 5, although the ratio of the nozzle exit area to the total base area is 0.1, there is a reasonable agreement between the CFD and multicomponent results.

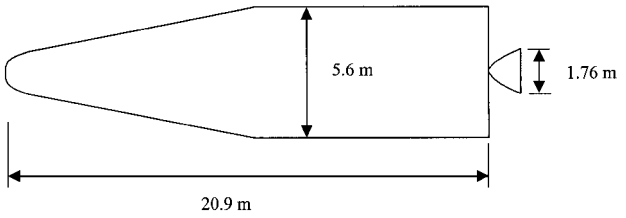

Fig. 5 Geometry used for computation of step 2.

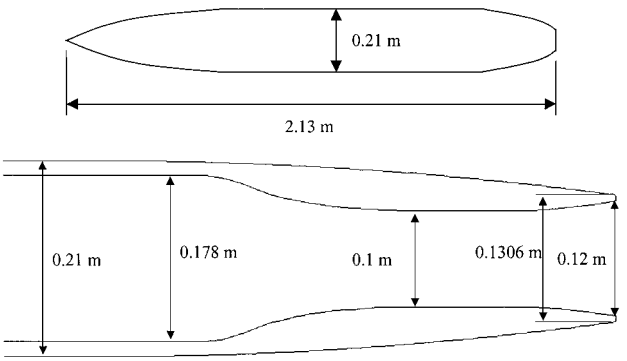

Fig. 6 Boattailed body and nozzle-base region.

Validation of Step 3

The plume-off case has been validated by comparing multicomponent method results with the results provided by Moore et al.,[36] which are reported in the review paper of Lamb and Oberkampf.[7] In this paper, a two-caliber tangent ogive nose with an aspect ratio, L/D, of 7.2 was considered at Mach 2 and 3 and at different angles of attack. Comparison of experimental and multicomponent method results is shown in Table 3.

In this case (plume-off), the multicomponent method provides results that are acceptable for engineering design purposes. The errors are smaller than 10% for angles of attack in the range from 0 to 8 deg, although away from this range, the accuracy quickly deteriorates. The reason, as pointed out by Lamb and Oberkampf,[7] is that at higher angles of attack the flow topology changes: The body vortex strength increases and a significant interaction takes place with the recirculating flow in the base cavity, thereby rendering invalid the assumptions on which the multicomponent method is built.

Validation of the plume-on cases has been carried out by comparing multicomponent method results with the experimental results of Englert et al.[31] The experimental model under consideration has a parabolic nose, a cylindrical centerbody, a boattailed section, and an exit-nozzle region. Its length is 2.13 m, and its maximum diameter 0.21 m. A schematic of the model is shown in Fig. 6. Detail of the

Table 3 Comparison between experimental and multicomponent method results: three-dimensional, perfect-gas, plume-off case

α, deg	$P_b(\alpha)/P_b(\alpha=0)$, experimental[36]	$P_b(\alpha)/P_b(\alpha=0)$, multicomponent	Error%, multicomponent
	$M_\infty = 2$		
0	1	1	0
2	0.94	0.92	2
4	0.84	0.84	0
6	0.75	0.74	1
8	0.68	0.65	4
10	0.63	0.52	17
12	0.58	0.44	24
	$M_\infty = 3$		
0	1	1	0
2	0.87	0.93	7
4	0.73	0.79	8
6	0.61	0.65	7
8	0.52	0.50	4
10	0.43	0.45	5

Table 4 Comparison between experimental and multicomponent method results: three-dimensional, perfect-gas, plume-on case

α, deg	P_b/P_∞, experimental[31]	P_b/P_∞, multicomponent	Error%, multicomponent
	$M_\infty = 2$, $NPR = 4$		
0	0.78	0.73	5
4	0.75	0.72	4
8	0.73	0.70	4
	$M_\infty = 2$, $NPR = 5$		
0	0.86	0.80	7
4	0.86	0.79	9
8	0.83	0.76	8

base region (including the internal dimensions of the nozzle) is also presented in Fig. 6. The external Mach number was 2, and nozzle pressure ratios of 4 and 5 were used for comparison. Table 4 shows the multicomponent results vs the experimental data. In this case, the errors associated with the multicomponent method are also acceptable for engineering design purposes. In particular, for the six cases that were considered, these errors were all smaller than 10%. Again, the error increased with the nozzle pressure ratio (NPR). CPU time was 7 min per case on a Pentium-based personal computer.

Results of Step 4

Because of the lack of wind-tunnel data that include simultaneous three-dimensional and real-gas effects, multicomponent results are presented without comparison with experimental tests. First, the geometry being studied was the one used in the validation of step 2 (Fig. 5), but considering a 5-deg angle of attack. External flow conditions, combustion chamber conditions, and C_p dependency with temperature are defined in the step 2 validation section. The computation at $\alpha = 5$ deg gave the value of 0.42 for P_b/P_∞ (remember that the value for the case with 0-deg angle of attack was 0.52). The trend of this result is in agreement with the trend for the case with a perfect gas shown in Table 4. That is, base pressure decreases when the angle of attack increases.

Second, the configuration used in the validation of step 3 section for plume-on conditions has been considered. In particular, it has been assumed that this missile-type body (Fig. 6) is powered by a stochiometric mixture of air and hexane (C_6H_{14}) with the following conditions: $M_\infty = 2$, NPR = 4 and 5, $P_T = 500$ kPa, and $T_T = 2000$ K. Accordingly, the following C_p variation was chosen: $C_p(T) = 926.8 + 0.449 \cdot T - 9.62 \times 10^{-5} \cdot T^2$ J/kg · K. The nozzle geometry is shown in Fig. 6. Comparison of perfect-gas and real-gas results in this three-dimensional, plume-on case is given in Table 5. Again, base pressure decreases, but only slightly, when the angle of attack increases. Also, in agreement with the discussion of Lamb and Oberkampf[7] on the effects of the ratio of specific heats, real-gas effects in the plume tend to decrease base pressure. CPU time in this case was of the order of 15 min on a Pentium-based personal computer for each simulation.

Table 5 Comparison between perfect-gas and real-gas multicomponent results: three-dimensional, plume-on case

α, deg	P_b/P_∞, multicomponent perfect gas	P_b/P_∞, multicomponent real gas
	$M_\infty = 2$, $NPR = 4$	
0	0.73	0.64
4	0.72	0.63
8	0.70	0.61
	$M_\infty = 2$, $NPR = 5$	
0	0.80	0.69
4	0.79	0.68
8	0.76	0.66

Conclusions

A multicomponent method has been formulated and validated, such that its accuracy and computational time requirements allow for its use as an engineering tool in practical design situations. In particular, because the method is able to simulate three-dimensional and real-gas effects its scope of applicability is broadened. Typical applications of interest are in the launcher and missile fields, both at the preliminary design level and at later stages by providing reliable startup solutions for CFD solvers.

The results of the validation study show that, within its parameter range of application, the accuracy of the multicomponent method is similar to (or even better than) that of sophisticated Reynolds averaged Navier–Stokes algorithms, at a fraction of their cost. Needless to say, the multicomponent method lacks the geometric and physics modeling flexibility that characterizes CFD applications. Regarding the simulation of three-dimensional and real-gas effects, the trend of the multicomponent results agrees with the experimental behavior observed by other authors. In particular, base pressure decreases (and drag increases) when the angle of attack increases and, also, when the ratio of specific heat is smaller than 1.4. This feature suggests that three-dimensional and real-gas effects should be accounted for as early as possible in the launcher and missile design processes because of their implication for vehicle and power plant sizing. Accordingly, that complex CFD simulations are still very costly and time consuming suggests the need to keep improving engineering and multicomponent methods, so that a reasonable blend of tools, of different accuracy and cost, is available to the design teams.

Acknowledgments

The authors are grateful to A. Sánchez, P. Rodríguez, and A. Lecuona at the Mechanical Engineering Department of Carlos III University of Madrid for their contribution to creating the environment that allowed for the completion of this study.

References

[1] Tang, H. H., and Barnes, J. W., "A Combining Parameter for Base Pressure Evaluation," *AIAA Journal*, Vol. 5, No. 9, 1967, pp. 1722–1724.

[2] Addy, A. L., "Experimental–Theoretical Correlation for Supersonic Jet-On Base Pressure for Cylindrical Afterbodies," *Journal of Aircraft*, Vol. 7, No. 5, 1970, pp. 474–477.

[3] Su, M. W., and Wu, J. M., "Base Pressure Correlation in Supersonic Flow," *AIAA Journal*, Vol. 9, No. 7, 1971, pp. 1429–1431.

[4] Kawecki, E. J., "Comparison of Several Re-Entry Vehicle Base Pressure Correlations," *Journal of Spacecraft*, Vol. 14, No. 5, 1977, pp. 284–289.

[5] Brazzel, C. E., and Henderson, J. H., "An Empirical Technique for Estimating Power-on Base Drag of Bodies of Revolution with a Single Jet Exhaust," CP-10, AGARD, 1966.

[6] Tanner M., "Theoretical Prediction of Base Pressure for Steady Base Flows," *Progress in Aerospace Sciences*, Vol. 14, 1973, pp. 177–225.

[7] Lamb, J. P., and Oberkampf, W. L., "Review and Development of Base Pressure and Base Heating Correlations in Supersonic Flow," *Journal of Spacecraft and Rockets*, Vol. 32, No. 1, 1995, pp. 8–23.

[8] Chapman, A. J., and Korst, H. H., "Free Jet Boundary with Consideration of Initial Boundary Layer," Second U.S. National Congress of Applied Mechanics, June 1954.

[9] Korst, H. H., Chow W. L., and Zumwalt G. W., "Research on Transonic and Supersonic Flow of a Real Fluid at Abrupt Increases in Cross-Section—Final Report," Mechanical Engineering Technical Rept. 392-5, Univ. of Illinois, Urbana, IL, Dec. 1959.

[10] Korst, H. H., "A Theory for Base Pressures in Transonic and Supersonic Flow," *Journal of Applied Mechanics*, Vol. 23, No. 4, 1956, pp. 593–600.

[11] Alber, I. E., and Lees, L., "Integral Theory for Supersonic Turbulent Base Flows," *AIAA Journal*, Vol. 6, No. 7, 1968, pp. 1343–1351.

[12] Fox, J. H., "Simple Recompression Model for the Korst Base Pressure Theory," *AIAA Journal*, Vol. 17, No. 3, 1979, pp. 311–313.

[13] Addy, A. L., Dutton, J. C., and Amatucci, V. A., "Nonuniform Nozzle Flow Effects on Base Pressure at Supersonic Flight Speeds," *AIAA Journal*, Vol. 24, No. 7, 1986, pp. 1209–1212.

[14] Schetz, J. A., Billig, F. S., and Favin, S., "Simplified Analysis of Supersonic Base Flows Including Injection and Combustion," *AIAA Journal* Vol. 14, No. 1, 1978, pp. 7, 8.

[15] Weng, C. H., and Chow, W. L., "Axisymmetric Supersonic Turbulent Base Pressure," *AIAA Journal*, Vol. 16, No. 6, 1978, pp. 553, 554.

[16] Tanner, M., "Boundary Layer Thickness and Base Pressure," *AIAA Journal*, Vol. 23, No. 12, 1985, pp. 1987–1989.

[17] Wagner, B., and White, R. A., "Supersonic Base Flow Problem in Presence of an Exhaust Jet," *AIAA Journal*, Vol. 18, No. 8, 1980, pp. 876–882.

[18] Hwang, C. B., Chow, W. L., and Moslemian, D., "Base Pressure of a Sudden Expansion from a Conical Converging Nozzle," *AIAA Journal*, Vol. 31, No. 4, 1993, pp. 657–662.

[19] Reijasse, P. R., Benay, R., Delery, J. M., and Lacau, R. G., "Missile and Projectile Base-Flow Prediction by Multicomponent Methods," AIAA Paper 88-4380, Aug. 1988.

[20] Delery J., and Wagner, B., "Results of Garteur Action Group AG09 on Flow Past Missile Afterbodies," *Missile Aerodynamics*, CP-493, AGARD, 1990, pp. 25-1, 25-35.

[21] Jenn, A., "Drag Prediction Methods for Axisymmetric Missile Bodies," *Tactical Missile Aerodynamics: Prediction Methodology*, Vol. 142, edited by M. R. Mendenhall, Progress in Astronautics and Aeronautics, AIAA, Washington, DC, 1991, pp. 37–62.

[22] Sahu, J., "Numerical Computations of Supersonic Base Flow with Special Emphasis on Turbulence Modelling," *AIAA Journal*, Vol. 32, No. 7, 1994, pp. 1547–1549.

[23] Chuang, C. C., and Chieng, C. C., "Supersonic Base-Flow Computation Using Higher-Order Closure Turbulence Models," *Journal of Spacecraft and Rockets*, Vol. 33, No. 3, 1996, pp. 374–380.

[24] Wang, T.-S., "Grid-Resolved Analysis of Base Flowfield for Four-Engine Clustered Nozzle Configuration," *Journal of Spacecraft and Rockets*, Vol. 33, No. 1, 1996, pp. 22–29.

[25] Sahu, J., and Heavey, K. R., "Numerical Investigation of Supersonic Base Flow with Base Bleed," *Journal of Spacecraft and Rockets*, Vol. 34, No. 1, 1997, pp. 62–69.

[26] Dash, S. M., and Sinha, N., "Exhaust Plumes and Their Interaction with Missile Airframes: A New Viewpoint," *Tactical Missile Aerodynamics: Prediction Methodology*, Vol. 142, edited by M. R. Mendenhall, Progress in Astronautics and Aeronautics, AIAA, Washington, DC, 1991, pp. 649–756.

[27] Sillen, M., "Investigation of Base Flow on a Space Rocket with Plumes," AIAA Paper 98-1599, April 1998.

[28] Matesanz, A., Velázquez, A., "EARSM Finite Element Solver for the Study of Turbulent 3-D Compressible Separated Flows," *Computer Methods in Applied Mechanics and Engineering*, Vol. 190, No. 8–10, 2000, pp. 989–1004.

[29] Délery, J., and Lacau, R.-G., "Prediction of Base Flows," *Special Course on Missile Aerodynamics*, AGARD Rept. 754, 1988.

[30] Mueller, J. S., Hall, C. R., Jr., and Roache, P. J., "The Influence of Initial Flow Direction on the Turbulent Base Pressure in Supersonic Axisymmetric Flow," *Journal of Spacecraft*, Vol. 7, No. 12, 1970, pp. 1484–1488.

[31] Englert, C. W., Vargo, D. J., and Cubbison, R. W., "Effect of Jet-Nozzle-Expansion Ratio on Drag of Parabolic Afterbodies," NACA RM E54B12, April 1959.

[32] Bannink, W. J., Houtmann, E. M., and Bakker, P. G., "Base Flow/Underexpanded Exhaust Plume Interaction in a Supersonic External Flow," AIAA Paper 98-1598, April 1998.

[33] Matesanz, A., Velázquez, A., Jiménez, A., and Rodríguez, M., "Numerically Robust 3-D Finite Element Reynolds Averaged Navier Stokes Solver for the Study of Turbulent Supersonic External Flows," *Computer Method in Applied Mechanics and Engineering*, No. 3–4, July 1998, pp. 383–394.

[34] Herrin, J. L., and Dutton, J. C., "Supersonic Base Flow Experiments in the Near Wake of a Cylindrical Afterbody," *AIAA Journal*, Vol. 32, No. 1, 1994, pp. 77–83.

[35] Herrin, J. L., and Dutton, J. C., "Supersonic Near-Wake Afterbody Boattailing Effects on Axisymmetric Bodies," *Journal of Spacecraft and Rockets*, Vol. 31. No. 6, 1994, pp. 1021–1027.

[36] Moore, F. G., Hymer, T., and Wilcox, F. J., "Improved Empirical Model for Base Drag Prediction on Missile Configurations Based on New Wind Tunnel Data," U.S. Naval Surface Warfare Center, Rept. NSWCDD/TR-92/509, Washington, DC, Oct. 1992.

R. M. Cummings
Associate Editor